

MS-RNN: A Flexible Multi-Scale Framework for Spatiotemporal Predictive Learning

Zhifeng Ma, Hao Zhang, and Jie Liu, *Fellow, IEEE*

Abstract—Spatiotemporal predictive learning, which predicts future frames through historical prior knowledge with the aid of deep learning, is widely used in many fields. Previous work essentially improves the model performance by widening or deepening the network, but it also brings surging memory overhead, which seriously hinders the development and application of this technology. In order to improve the performance without increasing memory consumption, we focus on scale, which is another dimension to improve model performance but with low memory requirement. The effectiveness has been widely proved in many CNN-based tasks such as image classification and semantic segmentation, but it has not been fully explored in recent RNN models. In this paper, learning from the benefit of multi-scale, we propose a general framework named Multi-Scale RNN (MS-RNN) to boost recent RNN models for spatiotemporal predictive learning. By integrating different scales, we enhance the existing models with both improved performance and greatly reduced overhead. We verify our MS-RNN framework by exhaustive experiments with 6 popular RNN models (ConvLSTM, TrajGRU, PredRNN, PredRNN++, MIM, and MotionRNN) on 4 different datasets (Moving MNIST, KTH, TaxiBJ, and HKO-7). The results show the efficiency that the RNN models incorporating our framework have much lower memory cost but better performance than before. Our code is released at <https://github.com/mazhf/MS-RNN>.

Index Terms—Spatiotemporal prediction, deep learning, RNN, scale.

I. INTRODUCTION

SPATIOTEMPORAL predictive learning, also known as video prediction learning, has aroused widespread research interest in the field of deep learning and computer vision. It benefits many aspects in real life, such as traffic flow prediction [1], [2], physical scene understanding [3]–[6], human motion trajectory prediction [7]–[10], robot control [11], [12], and precipitation nowcasting [13]–[17]. However, spatiotemporal prediction is an extremely challenging task, since motion always changes dramatically in both spatial and temporal domains. Therefore, how effectively learn the complex spatiotemporal transformations is the key issue for improving the model’s performance.

Since ConvLSTM [13] successfully learns the changes of the target object in space and time simultaneously by bringing convolutional operations into LSTM [19], a great deal of subsequent works have extended ConvLSTM by introducing well-designed modules. Essentially, they make the model

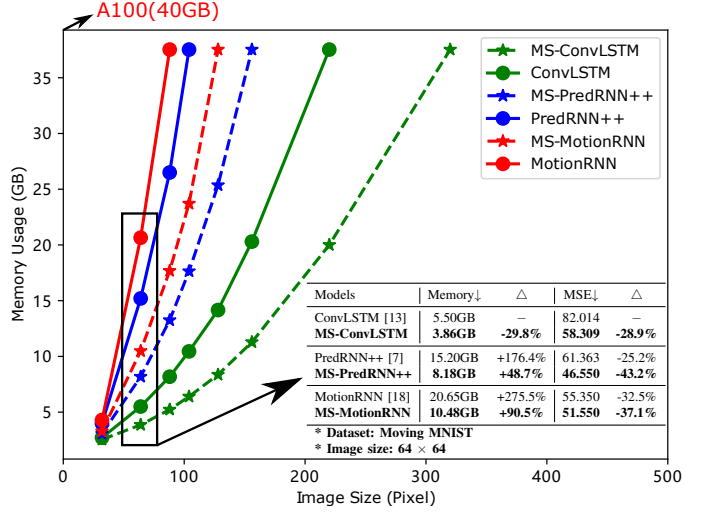


Fig. 1. Comparison of memory usage and performance of RNNs and MS-RNNs. Given a fixed image size, the memory footprint of advanced models (e.g., ConvLSTM → PredRNN++ → MotionRNN) is getting larger and larger. On the contrary, our proposed multi-scale framework can greatly reduce their memory footprint and brings additional improvement. Meanwhile, for a fixed memory footprint, our framework can make the basic models handle larger images, which expands the serviceable scope of the basic models. In addition, the performance of MS-ConvLSTM approaches the state-of-the-art MotionRNN. In practical applications, MS-ConvLSTM can be used to deal with high-resolution tasks (This paper adopts an RNN structure of 64 channels and 6 layers, which can be appropriately reduced to reduce memory usage to adapt to higher-resolution tasks (Section IV-B)).

wider (e.g., TrajGRU [14], PredRNN [7], MIM [15], and SA-ConvLSTM [10]) or deeper (e.g., PredRNN++ [9] and MotionRNN [18]). As a result, they bring limited improvement in model performance but introduce significant growth in GPU memory usage. For example in Fig. 1, compared with ConvLSTM, PredRNN++ reduces Mean Square Error (MSE) by 25.2% but increases the memory usage by 176.4%. MotionRNN reduces MSE by 32.5% but consumes much more memory by 275.5%. However, the memory dedicated to training the neural network is limited and precious. 40 GB memory is the limit of most modern GPUs [20]. The image size they can cope with is gradually decreasing when allowed to occupy full memory. As illustrated in Fig. 1, ConvLSTM can handle images with a maximum size of 220×220 , while MotionRNN can only handle images with a maximum size of 80×80 . On the contrary, real-world applications typically require high-resolution results [21], [22]. For example, the size of the radar image is usually over 500×500 in precipitation

Corresponding author: Hao Zhang (e-mail: zhh1000@hit.edu.cn)

Zhifeng Ma and Hao Zhang, Faculty of Computing, Harbin Institute of Technology, Harbin, 150001, China.

Jie Liu, International Institute for Artificial Intelligence, Harbin Institute of Technology, Shenzhen, 518055, China.

nowcasting, and the resolution of the front camera is larger than 1000×1000 pixels in the autonomous driving scenario. To fill this gap, the data has to be downsampled to reduce the memory footprint of the model in practice, which inevitably leads to the loss of details of the predicted frame and cannot meet the application requirements. Therefore, widening or deepening the model to improve the performance is not an optimal choice, since it leads to a sharp increase in memory consumption.

We aim to improve the performance without increasing memory consumption. In the computer vision domain, besides depth and width, there are two other dimensions that can improve performance, that is cardinality [23] and scale [24]. Cardinality reduces the number of parameters by grouping convolutions and then increases the number of groups to improve the performance while ensuring the same parameters as the original convolution. Unfortunately, cardinality also aggravates the memory footprint like width and depth. Obtaining multi-scale representations in vision tasks requires feature extractors to use a large range of receptive fields to describe objects at different scales [24], which can be achieved by stacking convolutional layers, using larger convolution kernels [25], or using pooling (downsampling) [26]. Among them, pooling is the most efficient way. In detail, the former two increase the depth and width of the network respectively, while the latter just adds some layers without parameters and allows the model to perform at low resolutions (low overhead). Unsurprisingly, multi-scale structures have long been adopted in image classification and semantic segmentation, and object detection domains, such as LeNet [27], AlexNet [28], VGGNet [29], UNet [30], FPN [31], etc. However, due to the complexity of the video prediction task, few works apply this structure to RNN models efficiently.

In this paper, we re-enable multiscale technology and propose a general framework named Multi-Scale RNN (MS-RNN) to improve existing RNN models. It should be emphasized that things are not as simple as directly migrating the multi-scale structures from convolutional models. First, we rearrange the tensor propagation flow of these increasingly complex RNN models and integrate them into a unified framework. Then we perform downsampling and upsampling processing for the tensors propagate along layers and times axes to get the multi-scale representations. Finally, we add skip connections between same-scale layers to get the MS-RNN framework. In addition, we also analyze the reasons for the overhead reduction and performance improvement brought by multi-scale structure: Mainly due to the reduction of outputs memory and increase of the spatiotemporal receptive field. MS-RNN performs excellently in the experiments. For instance, as shown in Fig. 1, compared with MotionRNN, MS-MotionRNN (MotionRNN using the MS-RNN framework) has better performance (reduce MSE from 55.35 to 51.55), while has much less memory overhead (reduce memory from 20.65GB to 10.48GB), which is almost half of vanilla MotionRNN. In summary, our contributions are as follows:

- We propose a general multi-scale framework named MS-RNN to improve the model performance and reduce the memory overhead meanwhile. It is compatible with

plenty of existing popular models such as ConvLSTM, TrajGRU, PredRNN, PredRNN++, MIM, and MotionRNN.

- We summarize and analyze the reasons for memory reduction and performance improvement when applying the multi-scale technique to RNN models.
- We verify the effectiveness of MS-RNN on 4 datasets and 6 typical models. All the results show that the recurrent models with our framework have much lower memory costs but higher performance than before.

II. RELATED WORK

Categories of Video Prediction Models. The mainstream video prediction models can be divided into three categories: Convolutional Neural Network (CNN), Recurrent Neural Network (RNN), and Generative Network [22]. A common 2D convolutional model is UNet [30], [32]. STConvS2S [33] introduces 3D convolution to try to make up for the lack of 2D convolution in capturing temporal trends. Subsequent series of RNN literature are based on ConvLSTM [13], such as TrajGRU [14], PredRNN [7], PredRNN++ [9], E3D-LSTM [8], MIM [15], CubicLSTM [34], SA-ConvLSTM [10], MotionRNN [18], and so on. However, these variants of ConvLSTM are increasingly complex, with a large number of parameters and memory occupation, and do not take into account the benefits of scale. Besides these deterministic prediction models, generative models explore the prediction problem by modeling the future uncertainty [35]. These models are either based on adversarial training (GAN) [26], [36] or variational autoencoders (VAEs) [37], [38] or both [39].

Multiscale Models in Video Prediction Task. In fact, multi-scale architectures are commonly used in the video prediction domain, such as RainNet [32], [26], SV2P [40], MCnet [41], [42], FitVid [43], and BP-Net [37]. However, these models either only use convolutions to construct multi-scale structures, use a ConvLSTM as the bottleneck layer between convolutional encoder and decoder, or use the first two structures in GANs or VAEs. These are different from the architecture proposed in this paper, MS-RNN improves models that have stacked RNN blocks. Stacking RNN layers is more powerful than stacking convolutional layers or a mix of the two. It is the reason why subsequent ConvLSTM variants such as PredRNN, PredRNN++, MIM, and MotionRNN use the stacked RNN structure, and why these models make improvements between RNN layers. For example, PredRNN introduces the spatiotemporal memory to ConvLSTM, which runs through the layers and propagates along a zigzag path. MIM adds a diagonal propagation path between the time axis and layers based on PredRNN. MotionRNN adds short-term and long-term memory between the layers of the MIM. The most similar to our work is [12], but using convolution and deconvolution for downsampling and upsampling brings additional parameters and memory usage. In addition, the difference between using multi-scale and invariant scale structures is not discussed, and experiments are only performed on ConvLSTM while our structure is compatible with a series of subsequent RNN models.

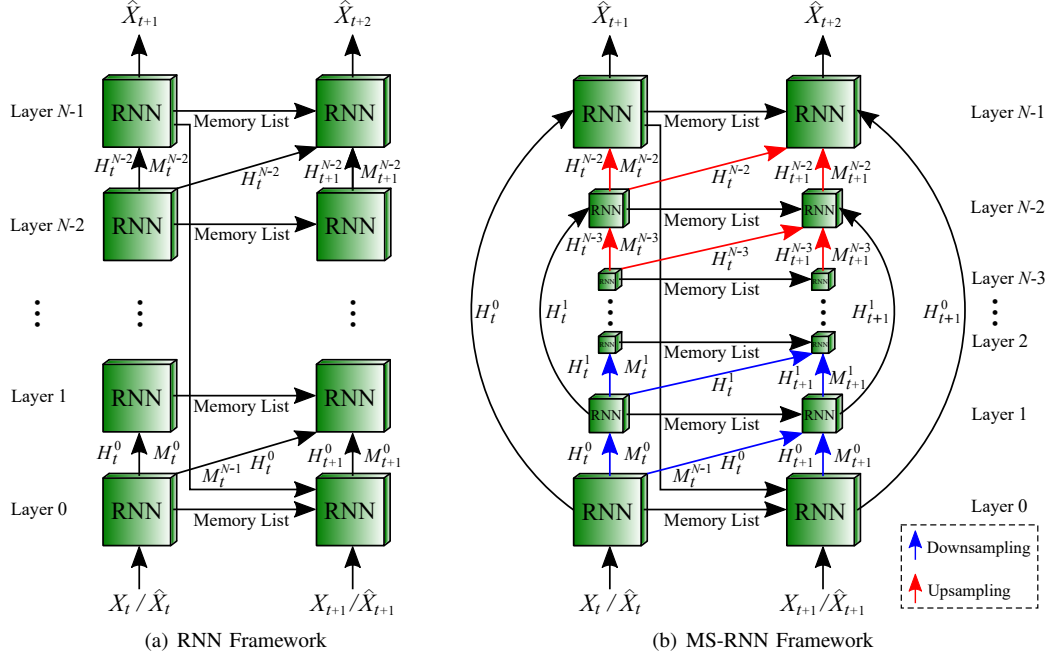


Fig. 2. First, we integrate ConvLSTM [13], TrajGRU [14], PredRNN [7], PredRNN++ [9], MIM [15], and MotionRNN [18] into a unified RNN framework with the same layers and complete tensor propagation path (a), and then perform multi-scale processing to get the MS-RNN framework (b). In detail, all models have the tensor H_t^l of time t and layer l that propagates along the vertical direction. Except for MS-ConvLSTM and MS-TrajGRU, all models have the tensor M_t^l that propagates along the zigzag direction. Only MS-MIM and MS-MotionRNN have the tensor H_{t-1}^{l-1} that propagates along the diagonal direction. All models have skip connections represented by curves to transfer the same scale features like H_t^0 and H_t^1 . The memory list propagates along the horizontal direction. For MS-TrajGRU, memory list = $[H_t^l]$. For MS-ConvLSTM, MS-PredRNN, and MS-PredRNN++, memory list = $[H_t^l, C_t^l, Z_t^l]$, and other layers have no memory Z_t^l . For MS-MIM, memory list = $[H_t^l, C_t^l, N_t^l, S_t^l, F_t^l, D_t^l]$.

III. PROBLEM FORMULATION

For a dynamical system (e.g., a video clip), from the spatial view, if we need to record C measurements of a certain local area ($H \times W$ grid points) at any time, we can express it in the form of a tensor $X_t \in \mathbb{R}^{C \times H \times W}$. To get a better picture of the 3D tensor, we can imagine them as vectors standing on a spatial grid. From the temporal view, we can express it as a sequence of tensors $\{X_0, \dots, X_{m-1}, X_m, \dots, X_{m+n-1}\}$. Let $X = \{X_0, \dots, X_{m-1}\}$ be the model input and $Y = \{X_m, \dots, X_{m+n-1}\}$ be the true target. The spatiotemporal predictive learning problem is to predict the most probable length- n prediction sequence \tilde{Y} in the future given the length- m observation sequence X . In this paper, we train a neural network parametrized by θ to solve such a task. We use stochastic gradient descent to find a set of parameters θ^* that maximizes the likelihood of producing the true target sequence Y given the input data X :

$$\theta^* = \arg \max_{\theta} P(Y|X; \theta). \quad (1)$$

IV. MS-RNN

A. Framework

Since Shi et al. [13] proposed the pioneer spatiotemporal prediction model named ConvLSTM, many variants of it have been proposed, which aim to solve the problem of the limited predictive ability of ConvLSTM. Unfortunately, although the

successors are more powerful, the essential reason for the improvement is making ConvLSTM deeper or wider, which results in a sharp increase in memory usage. Meanwhile, scale is an efficient dimension to both improve the model performance and reduce memory usage [44], but it is rarely adopted by these ConvLSTM variants in recent years. Motivated by this, we construct a general multi-scale framework for these models by introducing multi-scale layers into them. To fit all the existing popular models, we make uniform modifications in two aspects. First, we unify their structure and tensor flow into one RNN framework (Fig. 2(a)). Then we embed the multi-scale structure into the unified framework, forming the MS-RNN architecture (Fig. 2(b)). The structures of these models are similar but not totally the same. For example, PredRNN++ and MotionRNN have additional layers, and ConvLSTM and TrajGRU have no zigzag propagation path. We need to normalize them to make MS-RNN compatible with all models. Here we draw the most complex structure and the propagation path of all tensors in Fig. 2. It only needs to remove part of the propagation path and tensors when applying to other relatively simple models.

1) *Structure Unification*: The unified RNN framework is shown in Fig. 2(a), and different RNN models are compatible with this framework. Part of the tensors and propagation paths are optional, depending on the basic model used. Specifically, in the vertical direction, the hidden state H_t^l of time t and layer

l propagates along the stacked ConvLSTM layers for predicting the frame at the next moment; in the horizontal direction, H_t^l and the cell state C_t^l convey the memory of ConvLSTM of the previous moment. TrajGRU [14] brings optical flow into the hidden state, in which the recurrent connections are dynamically determined. Compared with ConvLSTM, it has only one memory H_t^l propagating along the horizontal direction. Compared with ConvLSTM, PredRNN [7] introduces an additional spatiotemporal memory cell M_t^l that propagates across zigzag directions. PredRNN++ [9] reorganizes the memories of PredRNN and adds a Gradient Highway Unit (GHU) between the first layer and the second layer, which we fuse with the second layer as one layer. Hence, the second layer of PredRNN++ has an additional memory Z_t^l flowing along the horizontal direction. Compared with PredRNN, MIM [15] introduces two memory cells (N_t^l and S_t^l) propagated in the horizontal direction to process non-stationary and stationary information, and a diagonal propagation path is added for differential H_t^{l-1} and H_{t-1}^{l-1} . MotionRNN [18] inserts the MotionGRU between the layers of MIM. For MotionGRU, we fuse it with the upper MIM layer into one layer. Hence, Compared with MIM, MotionRNN adds two memories (transient variation F_t^l and motion trends D_t^l) that propagate horizontally in each layer.

2) *Multi-scale Embedding*: Fig. 2(b) depicts the MS-RNN Framework. Unlike the RNN framework (Fig. 2(a)), downsampling (max pooling) and upsampling (bilinear interpolation) are added to construct a mirror pyramid structure, and skip connections (“+”) are added to combine the high-level semantic features and low-level detailed features of the same scales. In the vertical direction, only downsampling and upsampling H_t^l are required for MS-ConvLSTM and MS-TrajGRU. For MS-PredRNN, MS-PredRNN++, MS-MIM, and MS-MotionRNN, both H_t^l and M_t^l need to be sampled. In particular, for MS-MIM and MS-MotionRNN, sampling H_{t-1}^{l-1} along the diagonal propagation is also required. The scale of the memory in the memory list (Fig. 2) propagating along the horizontal direction remains the same for all models. The skip connection only transmits the output of the basic RNN (H_t^l). In principle, there are many choices of skip connection ways, such as similar to UNet 3+ [45] and fully connected ways, but experiments show that the one used in this paper is the simplest but the most effective (Table V).

B. Analysis of Memory Reduction

There are three main types of memory consumption in training the neural network [46], which are model memory, optimizer memory, and outputs memory. Model memory denotes the memory used to store the model parameters (\mathcal{M}_{par}). Optimizer memory refers to the memory used to store the parameters gradients and any momentum buffers during training. For Adam [47] (the most popular optimizer used in spatiotemporal predictive learning), the optimizer memory is 3x the model memory (i.e., $3\mathcal{M}_{par}$). Outputs memory denotes the memory occupied by the content of the forward and back propagations, which can be divided into forward outputs memory and backward outputs memory. Forward outputs memory

(\mathcal{M}_{out}) stores the outputs of each layer in the network for reuse in backpropagation. Backward outputs memory stores the gradients of outputs, whose size is equal to outputs [48]. Thus, the full memory overhead in training is

$$\mathcal{M}_{all} = 4\mathcal{M}_{par} + 2\mathcal{M}_{out}. \quad (2)$$

Suppose there are U basic units (such as input gates, forget gates, etc.) in the RNN module (the more complex the module, the larger the U). We denote the shape of the input or output tensor by (b, c, h, w) , the number of stacked layers of RNN by N (usually $N \geq 3$ for acceptable performance), and the number of recursion of RNN by R (equals to total sequence length $m + n$). Suppose the data type is the 32-bit floating-point. For the scale-invariant RNN model (Fig. 2(a)), the forward outputs memory usage is

$$\mathcal{M}_{out}^0 = 32RNUbchw \text{ bit}. \quad (3)$$

For the scale-variant RNN model (Fig. 2(b)), if N is odd, the forward outputs memory usage is

$$\begin{aligned} \mathcal{M}_{out}^1 &= 2 \times 32RUbc \left(hw + \frac{hw}{4} + \frac{hw}{16} + \cdots + \frac{hw}{4^{\frac{N-1}{2}}} \right) \\ &\quad + 32RUbc \times \frac{hw}{4^{\frac{N-1}{2}}} \\ &= \left(\frac{256}{3} \left(1 - \left(\frac{1}{4} \right)^{\frac{N-1}{2}} \right) + \frac{32}{4^{\frac{N-1}{2}}} \right) RUbchw \text{ bit}, \end{aligned} \quad (4)$$

and if N is even, we have

$$\begin{aligned} \mathcal{M}_{out}^1 &= 2 \times 32RUbc \left(hw + \frac{hw}{4} + \frac{hw}{16} + \cdots + \frac{hw}{4^{\frac{N-2}{2}}} \right) \\ &= \frac{256}{3} \left(1 - \left(\frac{1}{4} \right)^{\frac{N-2}{2}} \right) RUbchw \text{ bit}. \end{aligned} \quad (5)$$

Both \mathcal{M}_{out}^0 and \mathcal{M}_{out}^1 are monotonically increasing functions for N , and \mathcal{M}_{out}^1 is always smaller than \mathcal{M}_{out}^0 . Actually,

$$\begin{aligned} 96RUbchw \text{ bit} &\leq \mathcal{M}_{out}^0 \leq +\infty \text{ bit}, \\ 72RUbchw \text{ bit} &\leq \mathcal{M}_{out}^1 \leq \frac{256}{3} \approx 85RUbchw \text{ bit}. \end{aligned} \quad (6)$$

Since pooling, interpolation, and “+” do not introduce extra parameters, MS-RNN has the same parameters as RNN ($\mathcal{M}_{par}^1 = \mathcal{M}_{par}^0$). Therefore, compared to vanilla RNN, the memory overhead of MS-RNN is reduced by

$$\begin{aligned} \frac{\mathcal{M}_{all}^0 - \mathcal{M}_{all}^1}{\mathcal{M}_{all}^0} &= \frac{4\mathcal{M}_{par}^0 + 2\mathcal{M}_{out}^0 - 4\mathcal{M}_{par}^1 - 2\mathcal{M}_{out}^1}{4\mathcal{M}_{par}^0 + 2\mathcal{M}_{out}^0} \\ &= \frac{\mathcal{M}_{out}^0 - \mathcal{M}_{out}^1}{2\mathcal{M}_{par}^0 + \mathcal{M}_{out}^0} \\ &\stackrel{(1)}{\approx} \frac{\mathcal{M}_{out}^0 - \mathcal{M}_{out}^1}{\mathcal{M}_{out}^0}, \end{aligned} \quad (7)$$

where (1) holds for the fact that the outputs memory ($2\mathcal{M}_{out}$) is usually much larger than others memory ($4\mathcal{M}_{par}$) [46].

The memory footprint reduction is significant. For $N \geq 3$, the reduction is at least 25% ($N = 3$), theoretically. In practice, we usually use deeper networks for better performance.

For example, suppose we use the RNN with 6 layers (i.e., $N = 6$), the memory reduction is

$$\frac{\mathcal{M}_{all}^0 - \mathcal{M}_{all}^1}{\mathcal{M}_{all}^0} = \frac{192RUBchw - 84RUBchw}{2\mathcal{M}_{par}^0 + 192RUBchw} \approx 56.25\%. \quad (8)$$

In practice, this ratio varies according to different experiment settings (Section V). Different datasets and different basic RNN models result in different $RUBchw$, which determines the magnitude of \mathcal{M}_{out} and whether \mathcal{M}_{par} can be ignored. When $RUBchw$ is larger, the ratio of video memory reduction is closer to 56.25%.

C. Analysis of Performance Improvement

Limited by the scale of the convolution kernel, convolution can only capture the short-distance spatial dependence [26]. To obtain richer contextual information, the simplest one is stacking more convolution RNN layers, another way is introducing pooling layers between convolutional layers. Pooling makes the convolution kernel of the next layer see wider, i.e., wider spatiotemporal context information can be captured. However, pooling brings the loss of resolution, which has little impact on image or video classification tasks but is unacceptable for video prediction tasks, where the outputs and inputs have the same resolution. We solve this problem by using a mirror pyramid structure to restore resolution and join skip connections to preserve high-frequency information.

We analyze the efficiency of our framework by taking ConvLSTM with 6 layers as an example, where the first 3 layers can be regarded as an encoder for encoding the current frame, and the last 3 layers can be regarded as a decoder for decoding the next frame. The convolution operations in the input gate (i), output gate (o), forget gate (f), and modulation gate (g) is performed in parallel ($i, f, g, o = \sigma / \tanh(W_x * X_t + W_h * H_{t-1})$). Element-wise addition of input X_t after convolution and the hidden state H_{t-1} of the previous moment after convolution, element-wise addition and element-wise multiplication of the gating mechanism ($C_t = f \circ C_{t-1} + i \circ g$), as well as element-wise multiplication of final output ($H_t = o \circ \tanh(C_t)$), will not change the spatial receptive field obtained by convolution kernels. Theoretically, the receptive field of stacking 3 ConvLSTM layers is the same as that of stacking 3 convolution layers. In theory, stacking two 3×3 convolution layers has a receptive field equivalent to one 5×5 convolution layer, then the theoretical receptive field of the ConvLSTM encoder is 7×7 . However, the theoretical receptive field of the MS-ConvLSTM encoder will reach approximately 13×13 , because the receptive field of pooling combined with a 3×3 convolution is equivalent to a 6×6 convolution. Obviously, the MS-ConvLSTM encoder can capture longer-range spatiotemporal context than the ConvLSTM encoder, which will be of great help when modeling complex spatiotemporal changes. In addition, the poor performance of the ConvLSTM encoder also indirectly affects the effect of decoding prediction, while the MS-ConvLSTM decoder can obtain multi-scale context information from skip connections.

Furthermore, the use of multi-scale layers can capture the motion of objects of different scales, where the small scale

focuses on the contour and shape changes of the object, while the large scale focuses on some detailed features, such as the changes of clouds in a local area or the movement trajectories of hands and feet.

Table I. Training cost comparison and quantitative comparison on the Moving MNIST dataset. To speed up the training, we apply the Distributed Data Parallel (DDP) technology of Pytorch [49] to a single machine with four graphics cards. The table shows the memory occupation on one card, and the following results in other tables are also the same.

Models	Params	Memory	Δ	SSIM \uparrow	MSE \downarrow	MAE \downarrow
ConvLSTM [13]	1.77M	5.50GB	—	0.813	82.014	138.642
MS-ConvLSTM	1.77M	3.86GB	-29.8%	0.863	58.309	109.190
PredRNN [7]	3.59M	10.44GB	—	0.851	64.782	114.326
MS-PredRNN	3.59M	6.13GB	-41.3%	0.884	48.312	94.431
PredRNN++ [9]	5.61M	15.20GB	—	0.856	61.363	112.066
MS-PredRNN++	5.61M	8.18GB	-46.2%	0.892	46.550	89.307
MIM [15]	7.36M	19.69GB	—	0.861	58.634	109.885
MS-MIM	7.36M	10.09GB	-48.8%	0.884	48.593	93.637
MotionRNN [18]	7.56M	20.65GB	—	0.869	55.350	104.096
MS-MotionRNN	7.56M	10.48GB	-49.2%	0.882	51.550	97.103

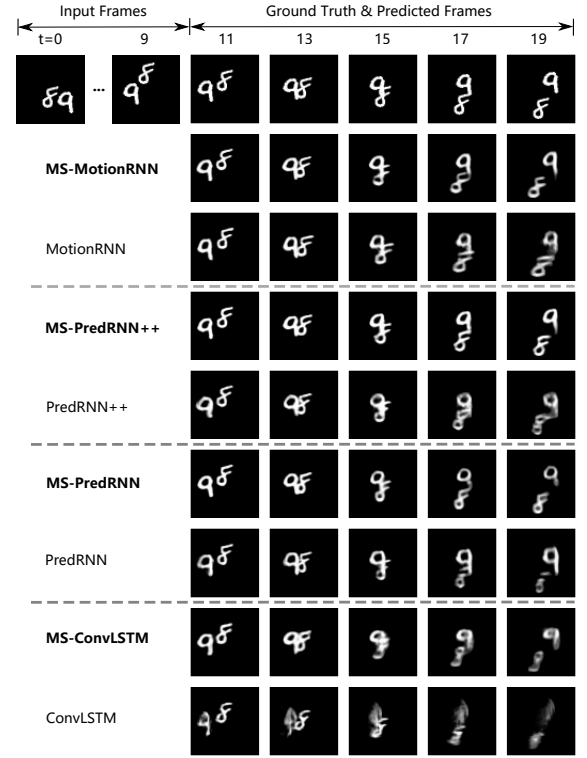


Fig. 3. Qualitative comparison on the Moving MNIST dataset.

V. EXPERIMENTS

We conduct experiments on a synthetic dataset (Moving MNIST) and three real-world datasets (TaxiBJ [2], KTH [50], HKO-7 [14]). Extensive experiments on these 4 datasets by 6 popular RNN models verify that our multi-scale architecture greatly reduces the memory footprint of the base models and improve their performance. On the one hand, the saved memory resource allows the models to handle larger images, which

broadens the application of the models. On the other hand, our framework enhance the performance of the base models, which will be of great help for the practical applications such as human trajectory prediction and precipitation nowcasting. Additionally, we also verify that both multiple scales and skip connections ways like UNet play important roles in our framework.

A. Implementation Details

To make fair comparisons, we apply the same experimental settings for all models. All models use a similar structure stacked with 6 layers of RNNs. We use Adam [47] as the optimizer and set the initial learning rate to 0.0003. We optimize the model with the $L_1 + L_2$ loss. In the training phase, the mini-batch is set to 4 for all datasets, and the training process is stopped after 30 epochs for HKO-7 and 20 epochs for other datasets. The kernel size of RNN is 3 and the channel of the hidden state is 64. The scheduled sampling strategy [51] is also adopted in the training process to guide the model to gradually learn the sample sequence features and reduce the differences between the training and testing stages. All experiments are tested on NVIDIA Tesla A100 GPU with 4 graphics cards of 40GB memory.

B. Moving MNIST

We generate Moving MNIST in the same way as [52]. The dataset contains a total of 15,000 sequences, and the sample ratio of the training set, validation set, and test set is 7 : 1 : 2. Each sequence contains 20 frames, 10 frames are used for training, and 10 frames are used for prediction. Each image in the sequence contains 2 numbers and the spatial size is 64×64 . The numbers in the training set and the test set are randomly obtained from the training and test set of the static MNIST dataset [27] respectively, such that the spatial information of the test data would not be overly exposed during the training process. These numbers bounce off the border at random positions, random speeds, and random directions. Although the extrapolation method of each sequence is fixed, the extrapolation method between different sequences is different.

From Table I, we can see that the parameters of multi-scale models remain consistent with basic models, but the memory cost of MS-MIM and MS-MotionRNN is almost half of the basic models. In addition, the multi-scale structure greatly improves the predictive ability of the basic models. For example, compared to ConvLSTM, the MSE of MS-ConvLSTM is reduced by 28.9% from 82.014 to 58.309. What's more surprising is that the mean performance of MS-ConvLSTM is even very close to that of the most advanced model MotionRNN.

The example in Fig. 3 is challenging because there is a severe occlusion in both the input sequence and the output sequence. Occlusion can be regarded as an information bottleneck, in which the mean and variance of the spatiotemporal process change drastically, indicating the existence of high-order non-stationarity [15]. Still, MS-RNNs produce clearer predictions, so we can conclude that multi-scale structure shows a strong ability in capturing non-stationary changes.

Table II. Training cost comparison and framewise comparison of MSE on the TaxiBJ dataset. The smaller MSE the better.

Models	Params	Memory	Δ	Frame 1	Frame 2	Frame 3	Frame 4
ConvLSTM [13]	1.77M	2.71GB	—	0.187	0.252	0.300	0.334
MS-ConvLSTM	1.77M	2.54GB	-6.3%	0.153	0.195	0.236	0.278
TrajGRU [14]	2.11M	3.51GB	—	0.179	0.255	0.306	0.350
MS-TrajGRU	2.11M	2.92GB	-16.8%	0.159	0.212	0.246	0.282
PredRNN [7]	3.59M	3.24GB	—	0.160	0.201	0.241	0.274
MS-PredRNN	3.59M	2.82GB	-13.0%	0.145	0.190	0.241	0.273
PredRNN++ [9]	5.61M	3.99GB	—	0.157	0.209	0.264	0.298
MS-PredRNN++	5.61M	3.07GB	-23.1%	0.155	0.208	0.254	0.294
MIM [15]	7.36M	4.16GB	—	0.152	0.202	0.250	0.287
MS-MIM	7.36M	3.24GB	-22.1%	0.151	0.197	0.244	0.280
MotionRNN [18]	7.56M	4.29GB	—	0.145	0.190	0.239	0.279
MS-MotionRNN	7.56M	3.28GB	-23.5%	0.142	0.185	0.219	0.251

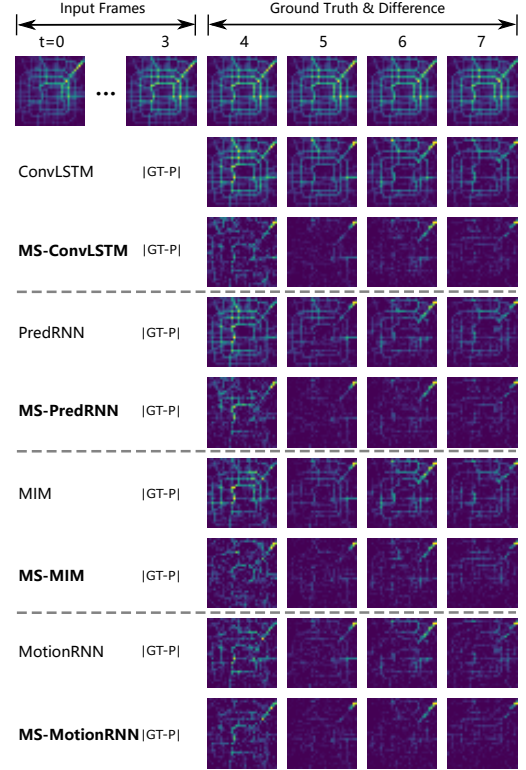


Fig. 4. Qualitative comparison on the TaxiBJ dataset. |GT-P| denotes the absolute difference frame between ground truth and predicted frames, prediction is the most accurate when there is nothing in the difference frame.

C. TaxiBJ Traffic Flow

The TaxiBJ dataset [2] contains taxicab trajectory data and meteorology data in four time periods in Beijing, which are collected by the sensors inside the cars. The trajectory data have two types of crowd flows, that is a $8 \times 32 \times 32 \times 2$ heat map, and the last dimension denotes the entering and leaving traffic flow intensities in the same area. We choose the entering traffic flow data for training. In detail, we use 4 known frames to predict the next 4 frames (traffic conditions for the next two hours). Then, we follow the experimental settings in MIM [15] and split the data into the training set and test set, in which the training set contains 19,560 samples while the test set contains 1,344 samples. In addition, we use the test set as the valid set.

As shown in Table II, the models that adopted multi-scale structures require less video card memory usage in the

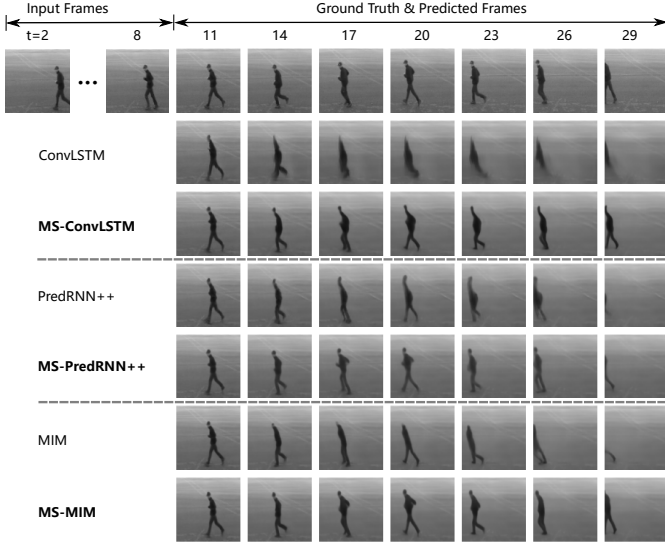


Fig. 5. Qualitative comparison on the KTH dataset.

training phase but have higher accuracy than basic models in the test phase. In addition, we also compare the absolute difference between the true images and the predicted images (Fig. 4). Obviously, the introduction of multi-scale technology improves the predictive ability of the basic models and reduces the prediction error.

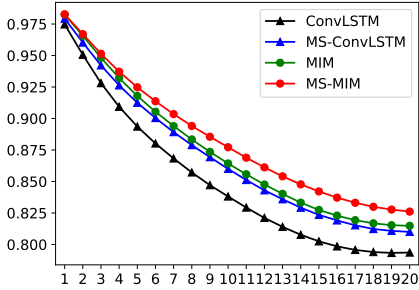


Fig. 6. Framewise SSIM comparison on the KTH dataset. The bigger SSIM the better.

D. KTH Human Action

The raw KTH dataset [50] contains six human actions (walking, jogging, running, boxing, hand waving, and hand clapping), performed by 25 subjects in four different scenarios: outdoors, outdoors with scale variations, outdoors with different clothes, and indoors. Currently, the dataset contains 2,391 video sequences. All sequences are shot on a homogeneous background using a static camera with a frame rate of 25fps. The sequence is downsampled to a spatial resolution of 160×120 pixels, with an average length of 4 seconds. We first save the video as pictures frame by frame, then resize the video frames into 88×88 pixels, and finally crop the frame based on the text provided in the dataset to ensure that humans always appear in the image. In this paper, we follow the experiment settings in PredRNN [7]. We use person 1-16

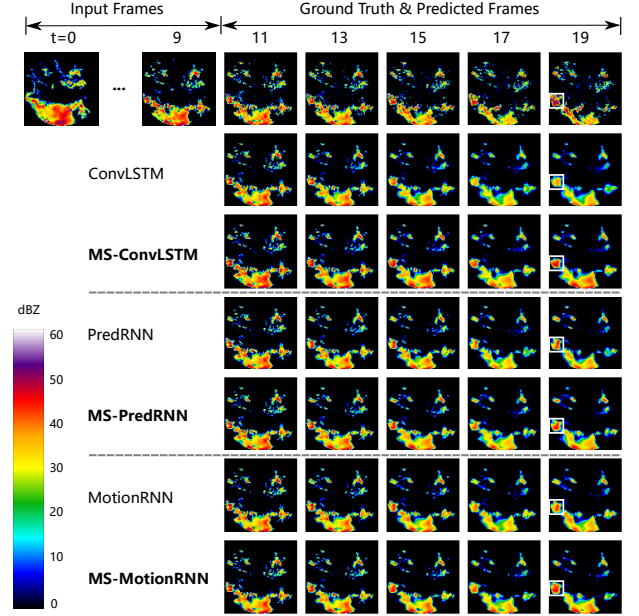


Fig. 7. Qualitative comparison on the HKO-7 dataset.

for training and 17-25 for testing (validation). In the training phase, the stride is 1 and the sliding window is 20. In the test phase, the stride for running and jogging is 3 while other actions are 20, and the sliding window is 30. Finally, 10 frames are used to predict the next 10 frames during training, and we extend the prediction horizon to 20 future time steps at test time.

Here we do not show training cost comparisons. Since the image size and total training sequence length of the KTH dataset are the same as that of HKO-7, the memory usage of these two datasets is similar (Table III). We use the quantitative metric Structural Similarity (SSIM [53]) to evaluate the quality of predicted frames. Fig. 6 shows the framewise comparisons of SSIM, which are obtained by calculating the average of all test sequences at each time step. Apparently, models with multiple scales yield better predictions than models without them. Fig. 5 also demonstrates this. From the examples in the figure, we can see that ConvLSTM, PredRNN++, and MIM produce ambiguous and distorted predictions, while MS-ConvLSTM, MS-PredRNN++, and MS-MIM produce clear and natural predictions. Among them, MS-MIM produces the best prediction results, which benefits from the application of multi-scale techniques. The large scales concern the movement of human body details such as arms and legs while the small scales care about the movement of the shape and contour of the human body.

E. Precipitation Nowcasting

For the HKO-7 dataset [14], only one Doppler radar is used to collect the data, and the radar echo map is collected from a height of 2km every 6 minutes. We only use rainy days data, with 812 days for training, 50 days for validation, and 131 days for testing. The raw radar images have a resolution of 480×480 pixels covering a 512×512 km area centered

Table III. Training cost comparison and quantitative comparison on the HKO-7 dataset.

Models	Params	Memory	Δ	CSI-0.5 \uparrow	CSI-5 \uparrow	CSI-30 \uparrow	HSS-0.5 \uparrow	HSS-5 \uparrow	HSS-30 \uparrow
ConvLSTM [13]	1.77M	8.18GB	—	0.741	0.629	0.321	0.837	0.757	0.441
MS-ConvLSTM	1.77M	5.23GB	-36.1%	0.746	0.632	0.343	0.841	0.761	0.466
PredRNN [7]	3.59M	18.05GB	—	0.750	0.645	0.370	0.844	0.770	0.504
MS-PredRNN	3.59M	9.64GB	-46.6%	0.754	0.647	0.375	0.847	0.773	0.511
PredRNN++ [9]	5.61M	26.50GB	—	0.748	0.643	0.364	0.842	0.769	0.495
MS-PredRNN++	5.61M	13.25GB	-50.0%	0.752	0.647	0.375	0.846	0.772	0.512
MIM [15]	7.36M	35.04GB	—	0.751	0.650	0.365	0.844	0.775	0.499
MS-MIM	7.36M	16.84GB	-52.0%	0.753	0.643	0.376	0.846	0.769	0.515
MotionRNN [18]	7.56M	37.53GB	—	0.752	0.642	0.357	0.846	0.767	0.491
MS-MotionRNN	7.56M	17.68GB	-52.9%	0.755	0.649	0.376	0.848	0.774	0.513

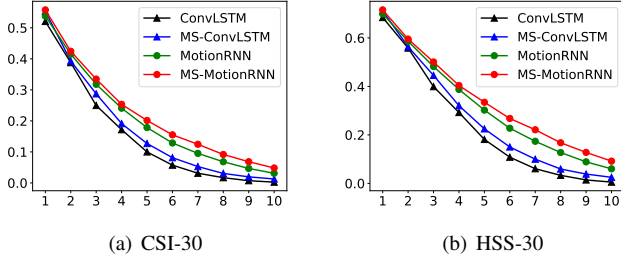


Fig. 8. Framework CSI-30 and HSS-30 comparison on the HKO-7 dataset.

in Hong Kong. We resize it to 88×88 pixels using bilinear interpolation.

We use the rainfall intensity thresholds 0.5, 5, and 30 mm/h to calculate the Critical Success Index (CSI) [14] and the Heidke Skill Score (HSS) [14]. Results are shown in Table III. In addition, we also compare the framewise CSI-30 and HSS-30 metrics of ConvLSTM and MotionRNN (Fig. 8), which focus on heavy rain that is more harmful to humans. Fig. 7 shows the qualitative results. We can see that the overall tone of the predictions of multi-scale methods is darker, and there is more attention being paid to the location of heavy rain. This is in line with the forecasting concept of weathermen, focusing mainly on rains with large areas of precipitation and high rainfall levels, ignoring those small areas of drizzles.

F. Ablation and Further Experiments

Table IV. Ablation study on the Moving MNIST dataset. The symbols w and w/o represent with and without respectively.

Models	Parts	Params	Memory	MSE \downarrow
ConvLSTM	w/o MS, w/o Skip	1.77M	5.50GB	82.014
MS-ConvLSTM	w MS, w/o Skip	1.77M	3.86GB	62.773
MS-ConvLSTM	w MS, w Skip	1.77M	3.86GB	58.309

We use ConvLSTM as the basic model to experiment with the effect of multi-scale structure and skip connection (UNet way). From Table IV, we can see that ConvLSTM's performance has been improved with the addition of them in sequence, and the memory usage has been reduced with the introduction of the multi-scale structure.

Furthermore, to investigate the efficiency of skip connection ways, we do more in-depth experiments on the skip connection

Table V. Comparison of different skip connection ways on the Moving MNIST dataset.

Models	Ways	Params	Memory	MAE \downarrow
MS-ConvLSTM	Fully Connected	1.77M	3.86GB	110.372
MS-ConvLSTM	UNet 3+	1.77M	3.86GB	109.504
MS-ConvLSTM	UNet	1.77M	3.86GB	109.190

settings using MS-ConvLSTM on the Moving MNIST dataset, such as similar to UNet 3+ [45] and fully connected way (Table V). The results show that the same-scale skip connection between encoder and decoder like UNet is the simplest but the most effective.

VI. CONCLUSIONS

In view of the problem that the dominant recurrent models try to solve spatiotemporal prediction issues occupy a large amount of memory, we propose a flexible and general framework named MS-RNN in this paper, which uses multi-scale technology to reduce the outputs memory during training. In addition, multi-scale technology also can capture the motion of objects of different scales, which is helpful for spatiotemporal modeling. Extensive experiments with 6 recurrent models on 4 tasks have demonstrated that models with MS-RNN have less memory usage but higher performance.

REFERENCES

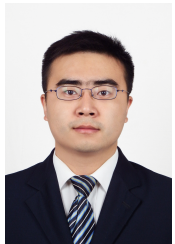
- [1] Z. Xu, Y. Wang, M. Long, J. Wang, and M. Kliss, "Predcnn: Predictive learning with cascade convolutions," in *International Joint Conference on Artificial Intelligence*, 2018, pp. 2940–2947.
- [2] J. Zhang, Y. Zheng, and D. Qi, "Deep spatio-temporal residual networks for citywide crowd flows prediction," in *AAAI Conference on Artificial Intelligence*, vol. 31, no. 1, 2017.
- [3] J. Wu, E. Lu, P. Kohli, B. Freeman, and J. Tenenbaum, "Learning to see physics via visual de-animation," *Advances in Neural Information Processing Systems*, vol. 30, 2017.
- [4] S. Van Steenkiste, M. Chang, K. Greff, and J. Schmidhuber, "Relational neural expectation maximization: Unsupervised discovery of objects and their interactions," *arXiv preprint arXiv:1802.10353*, 2018.
- [5] T. Kipf, E. Fetaya, K.-C. Wang, M. Welling, and R. Zemel, "Neural relational inference for interacting systems," in *International Conference on Machine Learning*. PMLR, 2018, pp. 2688–2697.
- [6] Z. Xu, Z. Liu, C. Sun, K. Murphy, W. T. Freeman, J. B. Tenenbaum, and J. Wu, "Unsupervised discovery of parts, structure, and dynamics," *arXiv preprint arXiv:1903.05136*, 2019.
- [7] Y. Wang, M. Long, J. Wang, Z. Gao, and P. S. Yu, "Predrnn: Recurrent neural networks for predictive learning using spatiotemporal lstm," *Advances in Neural Information Processing Systems*, vol. 30, 2017.
- [8] Y. Wang, L. Jiang, M.-H. Yang, L.-J. Li, M. Long, and L. Fei-Fei, "Eidetic 3d lstm: A model for video prediction and beyond," in *International Conference on Learning Representations*, 2018.

- [9] Y. Wang, Z. Gao, M. Long, J. Wang, and S. Y. Philip, "Predrnn++: Towards a resolution of the deep-in-time dilemma in spatiotemporal predictive learning," in *International Conference on Machine Learning*. PMLR, 2018, pp. 5123–5132.
- [10] Z. Lin, M. Li, Z. Zheng, Y. Cheng, and C. Yuan, "Self-attention convlstm for spatiotemporal prediction," in *AAAI Conference on Artificial Intelligence*, vol. 34, no. 07, 2020, pp. 11 531–11 538.
- [11] C. Finn and S. Levine, "Deep visual foresight for planning robot motion," in *IEEE International Conference on Robotics and Automation*. IEEE, 2017, pp. 2786–2793.
- [12] F. Ebert, C. Finn, A. X. Lee, and S. Levine, "Self-supervised visual planning with temporal skip connections," *arXiv preprint arXiv:1710.05268*, 2017.
- [13] X. Shi, Z. Chen, H. Wang, D.-Y. Yeung, W.-K. Wong, and W.-c. Woo, "Convolutional lstm network: A machine learning approach for precipitation nowcasting," *Advances in Neural Information Processing Systems*, vol. 28, 2015.
- [14] X. Shi, Z. Gao, L. Lausen, H. Wang, D.-Y. Yeung, W.-k. Wong, and W.-c. Woo, "Deep learning for precipitation nowcasting: A benchmark and a new model," *Advances in Neural Information Processing Systems*, vol. 30, 2017.
- [15] Y. Wang, J. Zhang, H. Zhu, M. Long, J. Wang, and P. S. Yu, "Memory in memory: A predictive neural network for learning higher-order non-stationarity from spatiotemporal dynamics," in *IEEE Conference on Computer Vision and Pattern Recognition*, 2019, pp. 9154–9162.
- [16] Y. Wang, H. Wu, J. Zhang, Z. Gao, J. Wang, P. Yu, and M. Long, "Predrnn: A recurrent neural network for spatiotemporal predictive learning," *IEEE Transactions on Pattern Analysis and Machine Intelligence*, 2022.
- [17] C. K. Sønderby, L. Espeholt, J. Heek, M. Dehghani, A. Oliver, T. Salimans, S. Agrawal, J. Hickey, and N. Kalchbrenner, "Metnet: A neural weather model for precipitation forecasting," *arXiv preprint arXiv:2003.12140*, 2020.
- [18] H. Wu, Z. Yao, J. Wang, and M. Long, "Motionrnn: A flexible model for video prediction with spacetime-varying motions," in *IEEE Conference on Computer Vision and Pattern Recognition*, 2021, pp. 15 435–15 444.
- [19] S. Hochreiter and J. Schmidhuber, "Long short-term memory," *Neural Computation*, vol. 9, no. 8, pp. 1735–1780, 1997.
- [20] F. Cheng, M. Xu, Y. Xiong, H. Chen, X. Li, W. Li, and W. Xia, "Stochastic backpropagation: A memory efficient strategy for training video models," in *IEEE Conference on Computer Vision and Pattern Recognition*, 2022, pp. 8301–8310.
- [21] S. Ravuri, K. Lenc, M. Willson, D. Kangin, R. Lam, P. Mirowski, M. Fitzsimons, M. Athanassiadou, S. Kashem, S. Madge *et al.*, "Skillful precipitation nowcasting using deep generative models of radar," *Nature*, 2021.
- [22] S. Oprea, P. Martinez-Gonzalez, A. Garcia-Garcia, J. A. Castro-Vargas, S. Orts-Escolano, J. Garcia-Rodriguez, and A. Argyros, "A review on deep learning techniques for video prediction," *IEEE Transactions on Pattern Analysis and Machine Intelligence*, 2020.
- [23] S. Xie, R. Girshick, P. Dollár, Z. Tu, and K. He, "Aggregated residual transformations for deep neural networks," in *IEEE Conference on Computer Vision and Pattern Recognition*, 2017, pp. 1492–1500.
- [24] S.-H. Gao, M.-M. Cheng, K. Zhao, X.-Y. Zhang, M.-H. Yang, and P. Torr, "Res2net: A new multi-scale backbone architecture," *IEEE Transactions on Pattern Analysis and Machine Intelligence*, vol. 43, no. 2, pp. 652–662, 2019.
- [25] C. Szegedy, W. Liu, Y. Jia, P. Sermanet, S. Reed, D. Anguelov, D. Erhan, V. Vanhoucke, and A. Rabinovich, "Going deeper with convolutions," in *IEEE Conference on Computer Vision and Pattern Recognition*, 2015, pp. 1–9.
- [26] M. Mathieu, C. Couprie, and Y. LeCun, "Deep multi-scale video prediction beyond mean square error," in *International Conference on Learning Representations*, 2016.
- [27] Y. LeCun, L. Bottou, Y. Bengio, and P. Haffner, "Gradient-based learning applied to document recognition," *Proceedings of the IEEE*, vol. 86, no. 11, pp. 2278–2324, 1998.
- [28] A. Krizhevsky, I. Sutskever, and G. E. Hinton, "Imagenet classification with deep convolutional neural networks," *Advances in Neural Information Processing Systems*, vol. 25, 2012.
- [29] K. Simonyan and A. Zisserman, "Very deep convolutional networks for large-scale image recognition," *arXiv preprint arXiv:1409.1556*, 2014.
- [30] O. Ronneberger, P. Fischer, and T. Brox, "U-net: Convolutional networks for biomedical image segmentation," in *International Conference on Medical Image Computing and Computer-assisted Intervention*. Springer, 2015, pp. 234–241.
- [31] T.-Y. Lin, P. Dollár, R. Girshick, K. He, B. Hariharan, and S. Belongie, "Feature pyramid networks for object detection," in *IEEE Conference on Computer Vision and Pattern Recognition*, 2017, pp. 2117–2125.
- [32] G. Ayzel, T. Scheffer, and M. Heistermann, "Rainnet v1. 0: a convolutional neural network for radar-based precipitation nowcasting," *Geoscientific Model Development*, vol. 13, no. 6, pp. 2631–2644, 2020.
- [33] R. Castro, Y. M. Souto, E. Ogasawara, F. Porto, and E. Bezerra, "Stconvs2s: Spatiotemporal convolutional sequence to sequence network for weather forecasting," *Neurocomputing*, vol. 426, pp. 285–298, 2021.
- [34] H. Fan, L. Zhu, and Y. Yang, "Cubic lstms for video prediction," in *AAAI Conference on Artificial Intelligence*, vol. 33, no. 01, 2019, pp. 8263–8270.
- [35] Z. Yao, Y. Wang, M. Long, and J. Wang, "Unsupervised transfer learning for spatiotemporal predictive networks," in *International Conference on Machine Learning*. PMLR, 2020, pp. 10 778–10 788.
- [36] S. Ravuri, K. Lenc, M. Willson, D. Kangin, R. Lam, P. Mirowski, M. Fitzsimons, M. Athanassiadou, S. Kashem, S. Madge *et al.*, "Skillful precipitation nowcasting using deep generative models of radar," *Nature*, vol. 597, no. 7878, pp. 672–677, 2021.
- [37] Y. Wang, J. Wu, M. Long, and J. B. Tenenbaum, "Probabilistic video prediction from noisy data with a posterior confidence," in *IEEE Conference on Computer Vision and Pattern Recognition*, 2020, pp. 10 830–10 839.
- [38] Z. Lin, C. Yuan, and M. Li, "Haf-svg: hierarchical stochastic video generation with aligned features," in *International Joint Conferences on Artificial Intelligence*, 2021, pp. 991–997.
- [39] R. Villegas, A. Pathak, H. Kannan, D. Erhan, Q. V. Le, and H. Lee, "High fidelity video prediction with large stochastic recurrent neural networks," *Advances in Neural Information Processing Systems*, vol. 32, 2019.
- [40] M. Babaeizadeh, C. Finn, D. Erhan, R. H. Campbell, and S. Levine, "Stochastic variational video prediction," *International Conference on Learning Representations*, 2018.
- [41] R. Villegas, J. Yang, S. Hong, X. Lin, and H. Lee, "Decomposing motion and content for natural video sequence prediction," *International Conference on Learning Representations*, 2017.
- [42] E. Denton and R. Fergus, "Stochastic video generation with a learned prior," in *International conference on machine learning*. PMLR, 2018, pp. 1174–1183.
- [43] M. Babaeizadeh, M. T. Saffar, S. Nair, S. Levine, C. Finn, and D. Erhan, "Fitvid: Overfitting in pixel-level video prediction," *arXiv preprint arXiv:2106.13195*, 2021.
- [44] H. Fan, B. Xiong, K. Mangalam, Y. Li, Z. Yan, J. Malik, and C. Feichtenhofer, "Multiscale vision transformers," in *IEEE International Conference on Computer Vision*, 2021, pp. 6824–6835.
- [45] H. Huang, L. Lin, R. Tong, H. Hu, Q. Zhang, Y. Iwamoto, X. Han, Y.-W. Chen, and J. Wu, "Unet 3+: A full-scale connected unet for medical image segmentation," in *IEEE International Conference on Acoustics, Speech and Signal Processing*. IEEE, 2020, pp. 1055–1059.
- [46] N. S. Sohoni, C. R. Aberger, M. Leszczynski, J. Zhang, and C. Ré, "Low-memory neural network training: A technical report," *arXiv preprint arXiv:1904.10631*, 2019.
- [47] D. P. Kingma and J. Ba, "Adam: A method for stochastic optimization," *arXiv preprint arXiv:1412.6980*, 2014.
- [48] Y. Gao, Y. Liu, H. Zhang, Z. Li, Y. Zhu, H. Lin, and M. Yang, "Estimating gpu memory consumption of deep learning models," in *ACM Joint Meeting on European Software Engineering Conference and Symposium on the Foundations of Software Engineering*, 2020, pp. 1342–1352.
- [49] A. Paszke, S. Gross, F. Massa, A. Lerer, J. Bradbury, G. Chanan, T. Killeen, Z. Lin, N. Gimelshein, L. Antiga *et al.*, "Pytorch: An imperative style, high-performance deep learning library," *Advances in Neural Information Processing Systems*, vol. 32, 2019.
- [50] C. Schuldt, I. Laptev, and B. Caputo, "Recognizing human actions: a local svm approach," in *International Conference on Pattern Recognition*, vol. 3. IEEE, 2004, pp. 32–36.
- [51] S. Bengio, O. Vinyals, N. Jaitly, and N. Shazeer, "Scheduled sampling for sequence prediction with recurrent neural networks," *Advances in Neural Information Processing Systems*, vol. 28, 2015.
- [52] N. Srivastava, E. Mansimov, and R. Salakhudinov, "Unsupervised learning of video representations using lstms," in *International conference on machine learning*. PMLR, 2015, pp. 843–852.
- [53] Z. Wang, A. C. Bovik, H. R. Sheikh, and E. P. Simoncelli, "Image quality assessment: from error visibility to structural similarity," *IEEE Transactions on Image Processing*, vol. 13, no. 4, pp. 600–612, 2004.

VII. BIOGRAPHY SECTION



Zhifeng Ma received his master's degree in Applied Statistics from Lanzhou University, Lanzhou, China, in 2020. He is currently pursuing a Ph.D. degree in Computer Science and Technology at Harbin Institute of Technology, Harbin, China. His research interests include deep learning, precipitation now-casting, and spatiotemporal predictive learning.



Hao Zhang received his Ph.D. degree in Information Security from University of Science and Technology of China, Hefei, China, in 2014. He is currently an Associate Researcher at Harbin Institute of Technology, Harbin, China. His research interests include deep learning application, federated learning, and pervasive computing.



Jie Liu (Fellow, IEEE) received his Ph.D. degree in Electrical Engineering and Computer Science from University of California, Berkeley, America, in 2001. He is currently a Chair Professor at Harbin Institute of Technology, Shenzhen, China. His research interests include artificial intelligence, control engineering, internet of things, and computer system.